6680 *Biochemistry* **2010,** *49,* 6680–6686
DOI: 10.1021/bi100929x

BIOCHEMISTRY
including biophysical chemistry & molecular biology
Article

Using Molecular Dynamics To Probe the Structural Basis for Enhanced Stability in Thermal Stable Cytochromes P450[†]

Yergalem T. Meharenna and Thomas L. Poulos*

Departments of Molecular Biology and Biochemistry, Chemistry, and Pharmaceutical Sciences, University of California, Irvine, California 92697-3900

Received June 9, 2010

ABSTRACT: High-temperature molecular dynamics (MD) has been used to assess if MD can be employed as a useful tool for probing the structural basis for enhanced stability in thermal stable cytochromes P450. CYP119, the most thermal stable P450 known, unfolds more slowly during 500 K MD simulations than P450s that melt at lower temperatures, P450cam and P450cin. A comparison of the 500 K MD trajectories shows that the Cys ligand loop, a critically important structural feature just under the heme, in both P450cin and P450cam completely unfolds while this region is quite stable in CYP119. In CYP119, this region is stabilized by tight nonpolar interactions involving Tyr26 and Leu308. The corresponding residues in P450cam are Gly and Thr, respectively. The in silico generated Y26A/L308A CYP119 double mutant is substantially less stable than wild-type CYP119, and the Cys ligand loop unfolds in a manner similar to that of P450cam. The MD thus has identified a potential "hot spot" important for stability. As an experimental test of the MD results, the Y26A/L308A double mutant was prepared, and thermal melting curves show that the double mutant exhibits a melting temperature (T_m) 16 °C lower than that of wild-type CYP119. Control mutations that were predicted by MD not to destabilize the protein were also generated, and the experimental melting temperature was not significantly different from that of the wild-type enzyme. Therefore, high-temperature MD is a useful tool in predicting the structural underpinnings of thermal stability in P450s.

Cytochromes P450 catalyze the hydroxylation of a wide range of substances and constitute one of Nature's largest enzyme families. Given the widespread occurrence of P450s throughout the biosphere, it was not too surprising when P450s were first discovered in thermophilic organisms (*1*). CYP119 from the acidothermophilic archaeon, *Sulfolobus acidocaldarius*, is the most thermal stable P450 known, with a melting temperature of ≈90 °C compared to a value of ≈55 °C for the well-known cytochrome P450cam (*2*, *3*). Given that P450s have the potential for catalyzing industrially and medically important hydroxylation reactions, an important goal is to understand the structural basis for such stability and then engineer the stability of CYP119 into the P450 of interest, thus generating a robust and useful catalyst. The crystal structure of CYP119 (*2*, *4*) revealed an unusual and extensive aromatic network not found in other P450s, which suggested that this may be one feature contributing to the stability of CYP119. Indeed, converting two of the Trp residues, at positions 4 and 281, involved in the aromatic stacking to Ala lowered the melting temperature by 15 °C (*5*), while a single Phe to Ser mutation lowered the T_m by ∼10 °C (*6*). Even so, many other comparative studies indicate several factors like salt bridges, shorter loops, and more compact packing contribute to enhanced stability (*7*).

In recent years, molecular dynamics (MD)[1] has emerged as an important tool in studying protein unfolding and stability (*8*−*14*). The main limitation is that the time scale of protein unfolding at room temperature is far too long for MD simulations of fully solvated protein models, but high-temperature MD in the range of 400−600 K accelerates the unfolding process to the nanosecond time range and thus can be accessed by MD (*10*, *15*, *16*). A detailed analysis of high-temperature versus low-temperature MD indicates that the unfolding path is not significantly different and that high-temperature MD in the range of 498 K over a shorter trajectory provides a realistic picture of stability and unfolding (*8*). Moreover, MD has been used successfully as a guide to determine the point at which to introduce mutations for the purpose of enhancing stability (*11*, *17*). Given these advances in the use of MD in studying stability and unfolding, we were encouraged to use similar approaches to try to understand the structural basis for stability in P450s. Here we report MD simulations for several P450s, including CYP119, coupled with experimental mutagenesis studies that reveal a heretofore, unexpected "hot spot" in P450s that is critically important in conferring enhanced stability.

EXPERIMENTAL PROCEDURES

MD Simulations. Although CYP119 is able to catalyze fatty acid hydroxylation in an artificially reconstituted monooxygenase system (*18*), the functional role of CYP119 remains unclear, and thus, there is no simple choice as to which P450 should serve as the mesophilic counterpart. Therefore, we chose P450cam and its close homologue P450cin. The structure of CYP119 has been determined with (*2*) and without (*4*) the ligand 4-phenylimidazole bound in the active site. There is a substantial difference in the two structures, with the ligand-free form having a wide open active site and the ligand-bound form being in a closed conformation. P450cam exhibits only the closed conformation with and without

[†]This work was supported by National Institutes of Health Grant GM33688.

*To whom correspondence should be addressed. E-mail: poulos@uci.edu. Telephone: (949) 824-7020. Fax: (949) 824-3280.

[1]Abbreviations: MD, molecular dynamics; rmsd, root-mean-square deviation.

 Published on Web 07/01/2010

a ligand bound (*19*). Therefore, we chose to compare the closed forms of both structures and started with the 4-phenylimidazole complexes of CYP119 [Protein Data Bank (PDB) entry 1F4T] and P450cam (PDB entry 1PHD) (*20*). Included in the P450s subjected to MD simulation were the 4-phenylimidazole complex of the thermally stable CYP231A2 (PDB entry 2FRC) from thermoacidophilic archaeon *Picrophilus torridus* (*21*), CYP175A1 (PDB entry 1N97) from *Thermus thermophilus* HB27 (*22*), and P450cin (PDB entry 1T2B) from *Citrobacter braakii* (*23*). For CYP175A1, an unknown ligand was found to be bound to the heme iron in the original structure determination so this was replaced with 4-phenylimidazole. Both CYP231A2 and CYP175A1 can be considered orphan P450s because the function of each remains unknown. Similarly, the substrate in P450cin was removed and 4-phenylimidazole modeled into the active site using the 4-phenylimidazole−P450cam complex as a guide. In this way, all P450s had the same ligand bound at the active site. P450cin was included as an additional mesophilic "control" because P450cin and P450cam are close homologues and were expected to behave similarly in high-temperature MD simulations.

The Amber 9.0 suite was used for all calculations (*24*). The ff99 force field provided with the Amber 9.0 package was used for the protein, while the heme-Cys ligand parameters were as described previously (*25*). Parameters for the 4-phenylimidazole were derived with Antechamber and the Gaff force field (*26*) using the BCC charging scheme (*27*, *28*). Ligands like phenylimidazole form a covalent bond with the iron, and this bond was constrained with a force constant of 200 kcal/Å to the 2.21 Å distance observed in the P450cam−4-phenylimidazole crystal structure. The angle defined by the Cys sulfur−heme Fe and 4-phenylimidazole N atom was 92° with a force constant of 10 kcal/Å. The P450 structures were stripped of crystallographic waters and then solvated with a box of TIP3 waters using a 10 Å cushion. Counterions were added to maintain a net neutral charge. The total numbers of atoms including explicit solvent for P450cam (CYP101), P450cin (CYP176A), CYP119, CYP231A2, and CYP175A1 were 36549, 39795, 41386, 31570, and 40069, respectively.

The structures were prepared for production MD runs by first energy minimization for 1000 cycles with all heavy atoms except water molecules fixed in position. This was followed by a short 10 ps MD run to allow just the water molecules to relax and 1000 cycles of energy minimization with all atoms allowed to move. Production runs for the 300 K 30 ns simulations were conducted with a 2 fs time step and coordinates saved every 10 ps. The temperature and pressure were held constant through weak coupling with a 1 ps pressure relaxation time and Langevin dynamics using a collision frequency of 1 ps^{-1}. Periodic boundary conditions were used with a particle mesh Ewald implementation of the Ewald sum for the description of long-range electrostatic interactions (*29*). A spherical cutoff of 8.5 Å was used for nonbonded interactions. Bonds involving hydrogen atoms were constrained using SHAKE (*30*). For the 500 K runs, the starting point was the end of the 30 ns 300 K trajectory. Trajectories were analyzed with the Ptraj program provided with the Amber 9.0 suite.

Simulations at 500 K were initiated from the final structure and velocities extracted from the 30 ns runs. It was necessary to run the 500 K simulations for only 8 ns because both P450cam and P450cin were substantially unfolded by 8 ns. Two methods were employed for simulations with mutants. In method 1, mutations were generated in silico by replacement of specific residues with Ala. The replacements were implemented by modifying the topology file and final frame of the 30 ns trajectory. Therefore, we start with an equilibrated structure and solvent box, thus avoiding a long 300 K simulation. The mutant structure was equilibrated for 1 ns at 300 K followed by an 8 ns 500 K run. In method 2, we started from the beginning and introduced the mutation into the crystal structure with a new solvent box followed by a full 30 ns 300 K simulation followed by 8 ns 500 K runs. There was no significant difference in the rmsd of backbone atoms using method 1 or 2. As a result, the "short cut" method 1 was employed.

Site-Directed Mutagenesis. The CYP119 expression plasmid was kindly provided by P. Ortiz de Montellano (University of California, San Francisco, CA). Mutations were introduced into the CYP119 gene, using the Stratagene (La Jolla, CA) QuikChange site-directed mutagenesis kit, and In-Fusion PCR cloning kit (Clontech). The primers required were obtained from Operon Technologies (Alameda, CA). The Y26A and L308A mutations were built into the wild-type (WT) Cyp119 gene individually. The following primers were used (positions of the mutations underlined): $Y26A_{for}$, TGG CAG GTG TTT TCC GCT AGG TAC ACA AAG G; $Y26A_{rev}$, C CTT TGT GTA CCT AGC GGA AAA CAC CTG CCA; $L308A_{for}$, CCG AAC CCA CAC GCA AGC TTT GGG TCT GG; $L308A_{rev}$, CC AGA CCC AAA GCT TGC GTG TGG GTT CGG. Once the mutant sequence of the Y26A was confirmed by DNA sequencing, it was used as a scaffold for the next step, where the L308A mutation was introduced using the same method, thereby generating the Y26A/L308A double mutant. The double mutation W147A/Y174A was introduced into the WT Cyp119 using oligos GATAAGGAGAAGTTCAAAGAG**GCG**TCAGACTTAGTCGCATTCAG (W147A) and GGTAAGAAGTACCTTGAGTTAATAGGT**GCT**GTGAAGGATCATCTAAATTCAG (Y174A) and the In-Fusion 2.0 dry-down PCR cloning kit. The sequences of all mutants were confirmed by DNA sequencing.

Expression and Purification. All of the proteins were expressed in *JM109DE3* cells. The mutant plasmids were transformed into *JM109* cells, and a single colony was selected for expression. The cells were grown in 2×YT (16 g/L tryptone, 10 g/L yeast extract, and 5 g/L NaCl) medium supplemented with 100 μg/mL ampicillin. Bacteria were grown to an optical density of 0.6 at 600 nm before protein expression was induced with 250 μM isopropyl β-D-thiogalactopyranoside (IPTG). Upon induction, the temperature was reduced to 26 °C, the shaking intensity was reduced to 80 rpm, and the cells were harvested 19 h after induction.

Cells were then lysed by sonication, but heat precipitation of the crude lysate was avoided; instead, the lysate was centrifuged at 17000*g* for 30 min, and the resulting clear supernatant was loaded onto a 20 mL Ni-NTA column. The column was washed with at least 10 column volumes of buffer containing 25 mM imidazole. Pure protein was eluted with 50 mM sodium phosphate buffer (pH 7.4) containing 100 mM imidazole. The red fractions were pooled and concentrated. Purity was confirmed by SDS−PAGE.

T_m Determination. The thermal melting temperatures were measured by following the absorbance of the heme Soret peak at a linear temperature rate of 0.5 °C/min on a Cary 3E UV−vis spectrophotometer equipped with a temperature controller. All measurements were taken in 50 mM sodium phosphate buffer (pH 7.4). All the reagents and enzymes necessary for site-directed mutagenesis were purchased from New England Biolabs Inc. (Beverly, MA), Invitrogen Corp. (Carlsbad, CA), and Qiagen Inc. (Valencia, CA). Chromatography columns were purchased from Qiagen Inc. All other chemicals were molecular biology grade.

Table 1: Average *B* Factors (Å^2) for Backbone Atoms

secondary structure	P450cam (CYP101)	CYP119	CYP231A2	CYP175A1
overall	17.6	18.8	17.4	17.20
C helix	17.9	18.2	10.8	8.9
D helix	28.7	17.5	11.9	12.3
E helix	11.9	8.4	5,7	7.9
F helix	**19.7**	**28.7**	**24.8**	**27.2**
G helix	**13.5**	**27.3**	**21.8**	**34.5**
H helix	15.7	25.1	18.1	23.7
I helix	6.9	8.7	9.4	9.3
J helix	13.3	15.1	31.0	9.5
K helix	8.9	6.6	5.9	4.5
L helix	15.5	11.6	9.1	5.2
***β* strands**	**7.2**	**13.1**	13.6	13.3
overall for secondary structure	14.5	16.4	15.6	14.2

RESULTS AND DISCUSSION

Room-Temperature MD. Each of the P450s, with the exception of P450cin, used in this study was subjected to 30 ns room-temperature MD simulations which was sufficient for equilibration as judged by stabilization of the rmsd (root-mean-square deviation) of backbone atoms (Figure S1 of the Supporting Information) from the starting crystal structures. P450cin was run for only 10 ns, but this was sufficient for equilibration.

Thermally stable proteins often are thought to be more rigid than their mesophilic counterparts, which is expected to be reflected in more rigidity during MD simulations. Atomic fluctuations thus were analyzed by computation of *B* factors for backbone atoms using snapshots from 12 to 30 ns. P450cin was not included in this analysis because room-temperature MD was run for only 10 ns. Table 1 provides the *B* factor for backbone atoms as a function of secondary structure, while Figure 1 highlights key helices in all P450s. Overall, there is little difference in *B* factor between the various P450s. A comparison between the MD and experimentally determined crystallographic *B* factors might be considered useful. However, in some of the crystal structures, surface helices, such as the F and G helices in P450cam, are involved in crystal contacts that tend to decrease *B* factors.

In addition to the overall *B* factors being very similar, the various elements of secondary structure also are similar. As expected, helical regions buried in the core of the protein or contacting the heme such as the I and L helices have low *B* factors. However, the F and G helices in all P450s exhibit higher *B* factors. The F and G helices and the connecting F−G loop are generally thought to undergo a large open−close motion in P450s which enables substrates to enter and products to leave. Note, however, that in the thermophilic P450s the F and G helices are more flexible than in P450cam. Another method for visualization of motions is to conduct a principal component analysis (*31*). Using Ptraj in Amber 9.0, the covariance matrix for Cα atoms computed over the last 20 ns of the simulation was diagonalized, thus providing a series of eigenvectors. Projection of these vectors onto the structure enables visualization of the primary low-frequency motions. Visualization was achieved using Interactive Essential Dynamics (*32*) and VMD (*33*). Movements along the first eigenvector in the region of the F and G helices are shown in Figure 2. It is clear that the F and G helices experience a greater range of motion in CYP119 than in P450cam. In agreement with these results, a much longer 200 ns MD simulation of CYP119 shows substantial motion of the region of helices F and G (*34*).

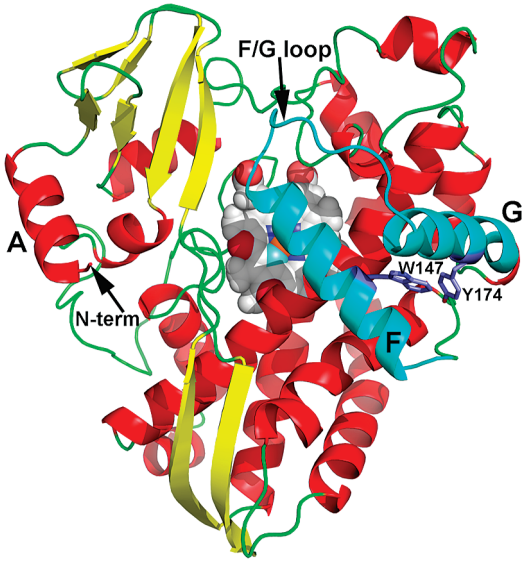

FIGURE 1: CYP119 with some key helices labeled. The F and G helices and the F−G loop are colored cyan. Also shown are two interacting aromatic residues, Trp147 and Tyr174.

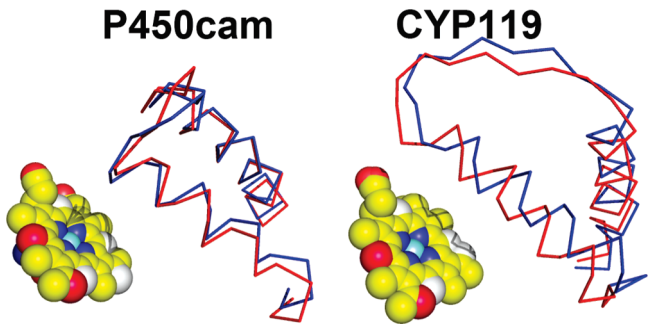

FIGURE 2: Regions of the F and G helices in P450cam and CYP119. The red and blue structures represent the extreme ends of the motion defined by the primary eigenvector obtained from the principal component analysis of the 300 K 30 ns MD trajectories.

The fact that CYP119 is actually more flexible in the region of helices F and G than P450cam while the rest of the structure is approximately as flexible as P450cam may at first seem counterintuitive since rigidity normally is associated with increased stability and is counter to the prevalent view that at room temperature, thermophilic proteins are more rigid and become flexible and functional only at elevated temperatures (*35*−*38*). However, an increasing number of both experimental and computational studies lead to a much different view. A recent neutron scattering experiment comparing *Escherichia coli* dihydrofolate reductase with its thermophilic counterpart found that the thermophilic enzyme is intrinsically more flexible (*39*). Similar conclusions were based on deuterium exchange experiments with α-amylases (*40*). MD simulations of diverse proteins (*9*, *12*, *14*, *41*) also came to the conclusion that the thermally stable proteins are no more rigid that their mesophilic cousins. Moreover, as noted by Lazaradis et al. (*42*), there is no thermodynamic advantage to rigidity. In fact, just the opposite may be true because greater flexibility in the folded protein means there is a smaller conformational entropic penalty in going from the unfolded to the folded state. It thus appears that CYP119 fits the pattern of not being more rigid than its mesophilic counterpart and in one region of the structure is actually more flexible.

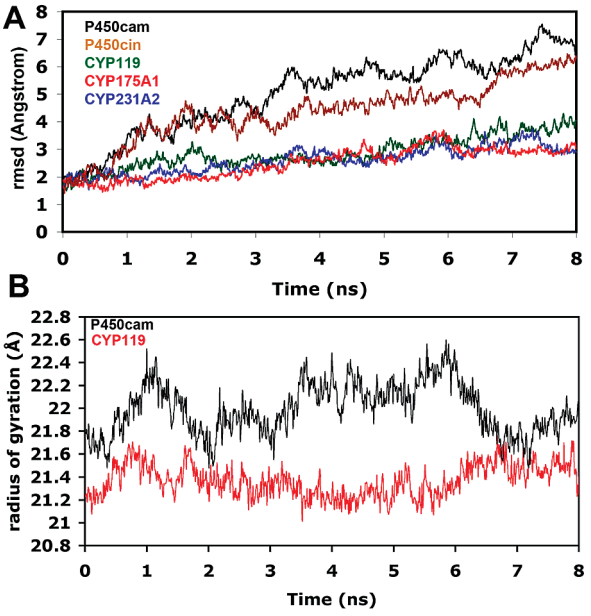

FIGURE 3: (A) rmsd values of backbone atoms (Cα, N, and C) for several P450s over the 8 ns trajectories at 500 K. (B) Radii of gyration for P450cam and CYP119 over the 8 ns 500 K trajectories.

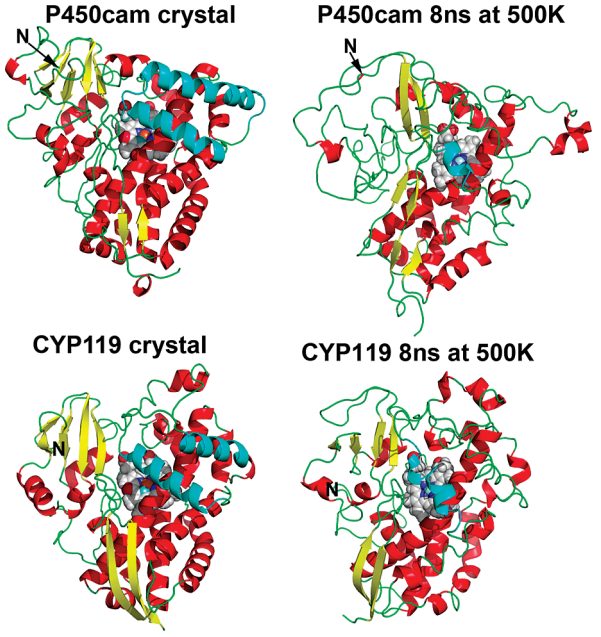

FIGURE 4: Models of the starting crystal structures and the last saved structure at 8 ns from the 500 K simulation.

High-Temperature MD. We next subjected the P450s to 500 K MD runs for 8 ns. We selected 500 K because previous studies have shown that 400−600 K is reasonable for following protein unfolding on the nanosecond time scale (*15*, *16*). The starting point was the end of the 30 ns 300 K simulation. The rmsd values from the starting crystal structures over the course of the unfolding trajectories are shown in Figure 3A, while Figure 3B shows the radii of gyration for P450cam and CYP119 as a function of time. As might be expected, P450cam and P450cin exhibit the largest rmsd over time, which indicates P450cam and P450cin are unfolding. There also is a greater variation and increase in the radius of gyration for P450cam compared to CYP119, indicative of a looser, less compact structure. This is more evident in Figure 4 which shows the 8 ns 500 K structures compared to the starting crystal structures. By 8 ns, both helices F and G are substantially unfolded in both P450s. However, in P450cam, the β structure in the top left region of the molecule (Figure 1) and helix A are unfolded, while in CYP119, the homologous region remains folded. Analysis of the 500 K trajectories also enables a quantitative estimate of the rate of secondary structure loss. In P450cam, ~40% of the helices are lost by 4 ns and 50% by 8 ns. In CYP119, ~20% of the helices are unfolded by 4 ns and 35% by 8 ns. We also checked the 500 K MD runs as a function of starting point. Others (*8*) have started from the energy-minimized crystal structure without first equilibrating the structure at 300 K. As shown in Figure S2 of the Supporting Information, there is essentially no difference between starting at the end of the 30 ns 300 K simulation or the energy-minimized crystal structure.

A closer view of some functionally important regions illustrates additional major differences between P450cam and CYP119. Figure 5 shows the Cys ligand loop found in all P450s. This is a β-bulge segment that forms a tight turn under the heme. Note that for CYP119 this region is very stable over the entire 8 ns at 500 K but completely unfolds in P450cam. We repeated the 500 K MD simulations by either taking velocities from the 20 ns 300 K MD structure rather than the 30 ns velocities or reinitializing with a new set of velocities. Either way, the Cys ligand loop unfolds in P450cam but remains stable in CYP119. One way of quantitating

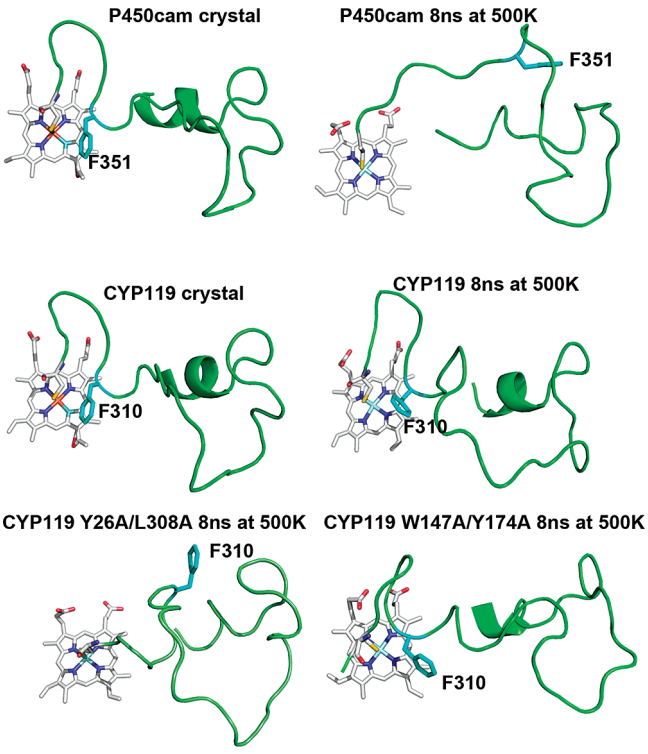

FIGURE 5: Beginning and ending structures from the 500 K simulations for P450cam, CYP119, and CYP119 mutants. Note that the Cys ligand loop completely unfolds in P450cam and the Y26A/L308A CYP119 mutant but not in wild-type CYP119 or the W147A/Y174A mutant.

this local unfolding is to follow the key hydrogen bond distance that helps to hold the Cys ligand loop together. All P450s have a hydrogen bond between the carbonyl O atom of the highly conserved Phe (cyan color in Figure 5) and the peptide NH group of the Cys ligand. This hydrogen bond distance is 2.9 Å in both P450cam and Cyp119 at the beginning of the 500 K MD runs. In P450cam, this distance increases to 18.1, 9.0, and 11.0 Å at the

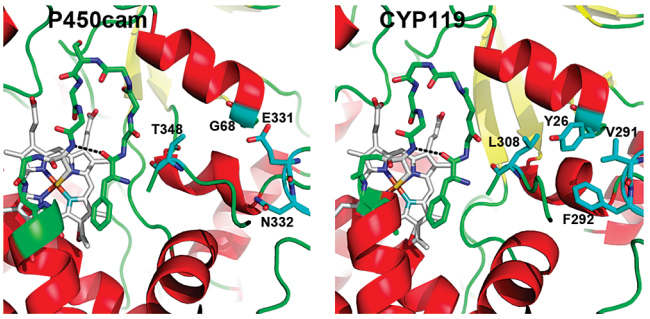

FIGURE 6: Detailed models of the Cys ligand loop in P450cam and CYP119.

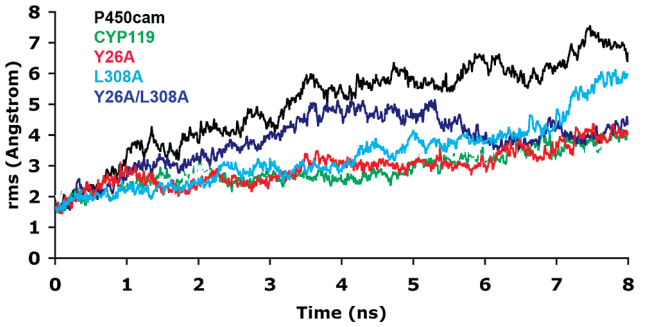

FIGURE 7: rmsd plots for the 8 ns trajectories at 500 K for CYP119, P450cam, and the in silico generated Y26A/L308A CYP119 mutant.

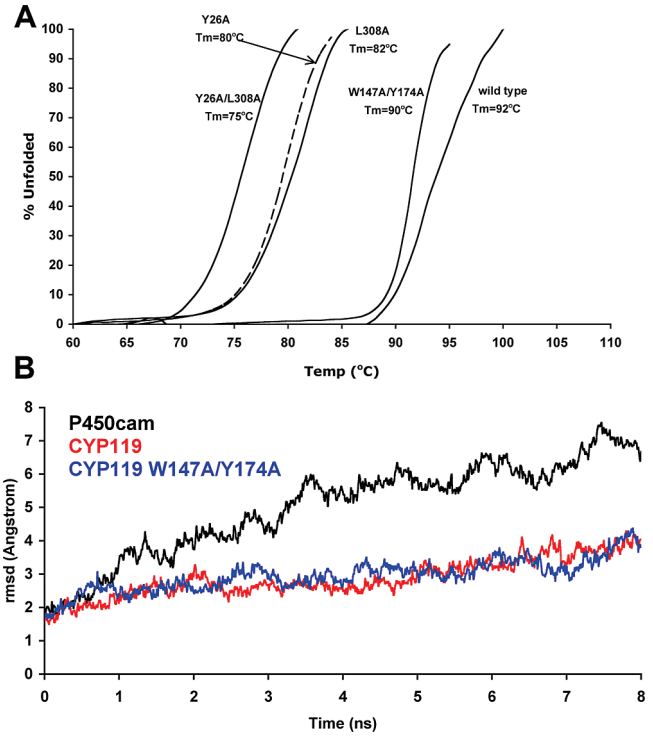

FIGURE 8: (A) Thermal melting curves for CYP119 and various mutants. On the *y*-axis, the minimum and maximum optical densities at 415 nm were normalized to 0 and 100, respectively. (B) rmsd plots for the 8 ns trajectories at 500 K for CYP119, P450cam, and the in silico generated W147A/Y174A CYP119 mutant.

end of the three 500 K MD runs, while in CYP119, the increase is to 3.1 Å in all three 500 K MD runs. The overall picture that emerges from these studies is one in which the helical core is fairly stable in P450s whereas the N-terminal region, the nearby β structure, and the Cys ligand loop are hot spots in P450cam and P450cin and unfold first during the 500 K simulation. We thus focused attention on these hot spot regions.

In Silico Mutagenesis. A closer examination of the Cys ligand loop provides some testable reasons for the differences in stability. As shown in Figure 6, P306, L308, F292, V291, and Y26 in CYP119 form a tight hydrophobic cluster at the N-terminal end of the Cys ligand loop. The corresponding residues in P450cam are T348, S346, N332, E331, and G68, respectively. This indicates the N-terminal region of the protein (Gly68 in P450cam and Tyr26 in CYP119) provides greater stability to the Cys ligand loop in CYP119. We already know from the MD work so far that a hot spot for early unfolding is the N-terminal part of the molecule. Therefore, as the N-terminal region unfolds, the Cys ligand loop is destabilized. In CYP119, the additional nonpolar interactions in this region provide additional stability.

To test this hypothesis, we generated in silico mutants of CYP119 and converted Tyr26 and Leu308, which form part of a tight cluster in CYP119 but not in P450cam, to Ala. We also generated the two single mutants. These mutants then were subjected to 500 K MD runs. The rmsd plots are shown in Figure 7. For comparison, P450cam and wild-type CYP119 are included. The double mutant unfolds more rapidly than wild-type CYP119 in a manner independent of the starting structure and velocities (Figure S3 of the Supporting Information). Not only is the double mutant substantially less stable than the wild type, but the Cys ligand loop unfolds like that of P450cam (Figure 5). It thus appears that the clustering of nonpolar residues ties the C-terminal end of the protein (Leu308) to the N-terminal end (Tyr26) and that the loss of this interaction results in substantial destabilization. The single mutants also unfold faster than the WT, but in both mutants, the Cys ligand loop remains intact at the end of the 500 K MD run.

Experimental Test. To test if Tyr26 and Leu308 indeed are important for stabilization, three mutants were generated: Y26A, L308A, and Y26A/L308A. These were purified and thermal melting curves determined (Figure 8A). The double mutant exhibits a T_m of 76 °C compared to 92 °C for wild-type CYP119, a significant 16 °C decrease in stability. The individual single mutants are more stable than the double mutant but still less stable than wild-type CYP119. We also conducted a control study by mutating two interacting nonpolar residues that were predicted by MD simulations not to alter stability. By visually examining the CYP119 structure, we selected Trp147 and Tyr174 as two interacting aromatic residues that are close together in sequence and should have little effect on stability. Moreover, these two residues form interactions between helices F and G (Figure 1) which are the two most flexible helices in the structure, and thus, mutations at these sites are likely to have little effect on stability. The 500 K MD run of the in silico generated W147A/Y174A double mutant predicts that these two mutations do not alter stability (Figure 8B). In addition, the Cys ligand loop does not unfold in this mutant (Figure 5). We also experimentally generated this mutant, and the thermal melting curve is shown in Figure 8A. The W147A/Y174A double mutant exhibits a T_m just a few degrees lower than that of the wild type. There thus is excellent agreement between the MD-predicted stability of mutants and experimental thermal melting curves.

CONCLUSION

The main goal of this study was to assess the use of MD simulations as a tool to help predict which regions of CYP119 might be especially important in conferring stability. What was not

evident in the static crystal structures, but suggested from MD, is that the Cys ligand loop region (Figure 3) and the tighter clustering on nonpolar groups in CYP119 are important for enhanced thermal stability, as compared to that of P450cam. It should be noted that this region is not part of the hydrophobic core of the protein and, in fact, Tyr26 and Leu308 are partially solvent exposed. Also noteworthy is the fact that the W4A/W281A double mutant melts at a temperature 15 °C lower than that of the wild type (*5*), and like Tyr26 and Leu308, these two Trp residues help to tie N- and C-terminal regions together in a partially exposed nonpolar cluster. The 500 K simulations show that the N-terminal region and the nearby β structure are particularly unstable at elevated temperatures, so perhaps one strategy CYP119 uses to enhance stability is to tether N- and C-terminal segments together via enhanced nonpolar interactions relative to P450cam. The experimental test of this prediction clearly shows that Tyr26 and Leu308 play important stabilization roles because converting these two groups to Ala lowered the T_m by ~16 °C.

The obvious next question is to ask if MD can be used to predict which mutants will increase stability. This is a much more challenging problem. For example, if we want to mimic the Tyr26−-Leu308 interaction found in CYP119 in P450cam, we would need to replace a Gly and Thr with larger nonpolar residues. This will cause other local and likely unfavorable packing problems. We did attempt to mimic the Tyr26−Leu308 interaction by introducing a S−S bond, but this mutant did not exhibit enhanced stability using the high-temperature MD test. Disulfide bonds, however, have highly restricted stereochemical requirements and are thus not likely to be generally useful for mimicking nonbonded intramolecular interactions. Salt bridges provide another possibility because there are far fewer stereochemical restraints, and given that such ionic interactions are on the surface, there is little problem with altering nonpolar packing. Indeed, in a study similar to ours, a salt bridge found to be important in the thermophilic protein was engineered into the mesophilic counterpart, resulting in enhanced stability of the mesophilic protein (*17*). It thus may be possible to mimic nonbonded intramolecular interactions that tie together residues distant in sequence with engineered salt bridges. In summary, this study illustrates that MD is a useful tool for predicting regions in P450s that are particularly important for conferring enhanced stability and perhaps can help streamline mutagenesis experiments.

ACKNOWLEDGMENT

We thank Prof. Rommie Amaro for valuable advice on MD simulations and for reading our manuscript.

SUPPORTING INFORMATION AVAILABLE

MD trajectories for 30 ns 300 K MD simulations and various control runs at 500 K. This material is available free of charge via the Internet at http://pubs.acs.org.

REFERENCES

1. Wright, R. L., Harris, K., Solow, B., White, R. H., and Kennelly, P. J. (1996) Cloning of a potential cytochrome P450 from the archaeon *Sulfolobus solfataricus*. *FEBS Lett*. *384*, 235–239.
2. Yano, J. K., Koo, L. S., Schuller, D. J., Li, H., Ortiz de Montellano, P. R., and Poulos, T. L. (2000) Crystal structure of a thermophilic cytochrome P450 from the archaeon *Sulfolobus solfataricus*. *J. Biol. Chem*. *275*, 31086–31092.
3. McLean, M. A., Maves, S. A., Weiss, K. E., Krepich, S., and Sligar, S. G. (1998) Characterization of a cytochrome P450 from the acidothermophilic archaea *Sulfolobus solfataricus*. *Biochem. Biophys. Res. Commun*. *252*, 166–172.
4. Park, S.-Y., Yamane, K., Adachia, S.-i., Shiro, Y., Weissb, K. E., Mavesb, S. A., and Sligar, S. G. (2002) Thermophilic cytochrome P450 (CYP119) from *Sulfolobus solfataricus*: High resolution structure and functional properties. *J. Inorg. Biochem*. *91*, 491–501.
5. Puchkaev, A. V., Koo, L. S., and Ortiz de Montellano, P. R. (2003) Aromatic stacking as a determinant of the thermal stability of CYP119 from *Sulfolobus solfataricus*. *Arch. Biochem. Biophys*. *409*, 52–58.
6. Maves, S. A., and Sligar, S. G. (2001) Understanding thermostability in cytochrome P450 by combinatorial mutagenesis. *Protein Sci. 10*, 161–168.
7. Petsko, G. (2001) Structural basis of thermosability in hyperthemophilic proeins, or "there's more than one way to skin a cat". *Methods Enzymol*. *334*, 469–478.
8. Day, R., Bennion, B. J., Ham, S., and Daggett, V. (2002) Increasing temperature accelerates protein unfolding without changing the pathway of unfolding. *J. Mol. Biol*. *322*, 189–203.
9. Grottesi, A., Ceruso, M. A., Colosimo, A., and Di Nola, A. (2002) Molecular dynamics study of a hyperthermophilic and a mesophilic rubredoxin. *Proteins 46*, 287–294.
10. Liu, J., Yu, H., and Shen, Z. (2008) Insights into thermal stability of thermophilic nitrile hydratases by molecular dynamics simulation. *J. Mol. Graphics Modell. 27*, 529–535.
11. Pikkemaat, M. G., Linssen, A. B., Berendsen, H. J., and Janssen, D. B. (2002) Molecular dynamics simulations as a tool for improving protein stability. *Protein Eng. 15*, 185–192.
12. Wintrode, P. L., Zhang, D. Q., Vaidehi, N., Arnold, F. H., and Goddard, W. A. (2003) Protein dynamics in a family of laboratory evolved thermophilic enzymes. *J. Mol. Biol. 327*, 745–757.
13. Colombo, G., and Merz, K. M. (1999) Stability and Activity of Mesophilic Subtilisin E and Its Thermophilic Homolog: Insights from Molecular Dynamics Simulations. *J. Am. Chem. Soc. 121*, 6895–6903.
14. Merkley, E. D., Parson, W. W., and Daggett, V. (2010) Temperature dependence of the flexibility of thermophilic and mesophilic flavoenzymes of the nitroreductase fold. *Protein Eng., Des. Sel. 23*, 327–336.
15. Huang, X. Q., and Zhou, H. X. (2006) Similarity and difference in the unfolding of thermophilic and mesophilic cold shock proteins studied by molecular dynamics. *Biophys. J. 91*, 2451–2463.
16. Purmonen, M., Valjakka, J., Takkinen, K., Laitinen, T., and Rouvinen, J. (2007) Molecular dynamics studies on the thermostability of family 11 xylanases. *Protein Eng. 20*, 551–559.
17. Bae, E., and Phillips, G. N., Jr. (2005) Identifying and engineering ion pairs in adenylate kinases. Insights from molecular dynamics simulations of thermophilic and mesophilic homologues. *J. Biol. Chem. 280*, 30943–30948.
18. Puchkaev, A. V., Wakagi, T., and Ortiz de Montellano, P. R. (2002) CYP119 plus a *Sultolobus tokodaii* strain 7 ferredoxin and 2-oxoacid: ferredoxin oxidoreductase constitute a high-temperature cytochrome P450 catalytic system. *J. Am. Chem. Soc. 124*, 12682–12683.
19. Poulos, T. L., Finzel, B. C., and Howard, A. J. (1986) Crystal structure of substrate-free *Pseudomonas putida* cytochrome P-450. *Biochemistry 25*, 5314–5322.
20. Poulos, T. L., and Howard, A. J. (1987) Crystal Structures of Metyrapone-Inhibited and Phenylimidazole-Inhibited Complexes of Cytochrome P-450cam. *Biochemistry 26*, 8165–8174.
21. Ho, W. W., Li, H., Nishida, C. R., Ortiz de Montellano, P. R., and Poulos, T. L. (2008) Crystal structure and properties of CYP231A2 from the thermoacidophilic archaeon *Picrophilus torridus*. *Biochemistry 47*, 2071–2079.
22. Yano, J. K., Blasco, F., Li, H., Schmid, R. D., Henne, A., and Poulos, T. L. (2003) Preliminary characterization and crystal structure of a thermostable cytochrome P450 from *Thermus thermophilus*. *J. Biol. Chem. 278*, 608–616.
23. Meharenna, Y. T., Li, H., Hawkes, D. B., Pearson, A. G., De Voss, J., and Poulos, T. L. (2004) Crystal structure of P450cin in a complex with its substrate, 1,8-cineole, a close structural homologue to D-camphor, the substrate for P450cam. *Biochemistry 43*, 9487–9494.
24. Case, D. A., Cheatham, T. E., Darden, T., Gohlke, H., Luo, R., Merz, K. M., Onufriev, A., Simmerling, C., Wang, B., and Woods, R. J. (2005) The Amber biomolecular simulation programs. *J. Comput. Chem. 26*, 1668–1688.
25. Harris, D. L., Park, J. Y., Gruenke, L., and Waskell, L. (2004) Theoretical study of the ligand-CYP2B4 complexes: Effect of structure on binding free energies and heme spin state. *Proteins 15*, 895–914.
26. Wang, J., Wolf, R. M., Caldwell, J. W., Kollman, P. A., and Case, D. (2004) Development and testing of a general Amber force field. *J. Comput. Chem. 25*, 1157–1174.

27. Jakalian, A., Bush, B. L., Jack, D. B., and Bayly, C. I. (2000) Fast, efficient generation of high-quality atom charges. AM1-BCC model: I. Method. *J. Comput. Chem. 21*, 132–146.
28. Jakalian, A., Jack, D. B., and Bayly, C. I. (2002) Fast, efficient generation of high-quality atom charges. AM1-BCC model: II. Parameterization and validation. *J. Comput. Chem. 23*, 1623–1641.
29. Darden, T., York, D., and Pedersen, L. (1993) Particle mesh Ewald: An Nlog(N) method for Ewald sums in large systems. *J. Chem. Phys. 103*, 8577–8593.
30. Miyamoto, S., and Kollman, P. A. (1992) SETTLE: An analytical version of the SHAKE and RATTLE algorithm for rigid water molecules. *J. Comput. Chem. 13*, 952–962.
31. Amadei, A., Linssen, A. B., and Berendsen, H. J. (1993) Essential dynamics of proteins. *Proteins 17*, 412–425.
32. Mongan, J. (2004) Interactive essential dynamics. *J. Comput.-Aided Mol. Des. 18*, 433–436.
33. Humphrey, W., Dalke, A., and Schulten, K. (1996) VMD: Visual molecular dynamics. *J. Mol. Graphics 14* (33−38), 27–38.
34. Lampe, J. N., Brandman, R., Sivaramakrishnan, S., and de Montellano, P. R. (2010) Two-dimensional NMR and all-atom molecular dynamics of cytochrome P450 CYP119 reveal hidden conformational substates. *J. Biol. Chem. 285*, 9594–9603.
35. Kohen, A., and Klinman, J. P. (2000) Protein flexibility correlates with degree of hydrogen tunneling in thermophilic and mesophilic alcohol dehydrogenases. *J. Am. Chem. Soc. 122*, 10738–10739.
36. Varley, P. G., and Pain, R. H. (1991) Relation between Stability, Dynamics and Enzyme Activity in 3-Phosphoglycerate Kinases from Yeast and *Thermus thermophilus*. *J. Mol. Biol. 220*, 531–538.
37. Wolf-Watz, M., Thai, V., Henzler-Wildman, K., Hadjipavlou, G., Eisenmesser, E. Z., and Kern, D. (2004) Linkage between dynamics and catalysis in a thermophilic-mesophilic enzyme pair. *Nat. Struct. Mol. Biol. 11*, 945–949.
38. Zavodszky, P., Kardos, J., Svingor, A., and Petsko, G. A. (1998) Adjustment of conformational flexibility is a key event in the thermal adaptation of proteins. *Proc. Natl. Acad. Sci. U.S.A. 95*, 7406–7411.
39. Meinhold, L., Clement, D., Tehei, M., Daniel, R., Finney, J. L., and Smith, J. C. (2008) Protein dynamics and stability: The distribution of atomic fluctuations in thermophilic and mesophilic dihydrofolate reductase derived using elastic incoherent neutron scattering. *Biophys. J. 94*, 4812–4818.
40. Fitter, J., and Heberle, J. (2000) Structural equilibrium fluctuations in mesophilic and thermophilic α-amylase. *Biophys. J. 79*, 1629–1636.
41. Tang, L., and Liu, H. (2007) A comparative molecular dynamics study of thermophilic and mesophilic ribonuclease HI enzymes. *J. Biomol. Struct. Dyn. 24*, 379–392.
42. Lazaridis, T., Lee, I., and Karplus, M. (1997) Dynamics and unfolding pathways of a hyperthermophilic and a mesophilic rubredoxin. *Protein Sci. 6*, 2589–2605.